THERMAL AND THERMOMECHANICAL BUCKLING OF CNT-REINFORCED COMPOSITE SANDWICH CYLINDRICAL SHELLS INCLUDING ELASTICITY OF TANGENTIAL EDGE RESTRAINT

Hoang Van Tung[1,*]**, Pham Thanh Hieu**[2]

[1]*Faculty of Civil Engineering, Hanoi Architectural University, Hanoi, Vietnam*
[2]*Faculty of Civil Engineering, University of Transport Technology, Hanoi, Vietnam*
*E-mail: tunghv@hau.edu.vn

Abstract. This paper presents an analytical approach to investigate the buckling of sandwich cylindrical shells subjected to uniform temperature rise and external lateral pressure. Two sandwich models corresponding to carbon nanotube reinforced composite (CNTRC) face sheets and core layer are considered. The properties of all constitutive materials are assumed to be temperature dependent and effective properties of CNTRC are determined according to an extended rule of mixture. Governing equations are established using first order shear deformation theory and solved employing two-term form of deflection along with Galerkin method for simply supported edge shells. In order to account for practical situations of in-plane boundary condition, the elasticity of tangential constraint of boundary edges is included. Owing to temperature dependence of material properties, critical thermal loads are determined adopting an iteration process. Numerous parametric studies are carried out and interesting remarks are given. The study reveals that sandwich shell model with CNTRC core layer and homogeneous skins has considerably strong capacity of buckling resistance. Numerical results also indicate that tangential edge constraint has significant effects on critical loads, especially at elevated temperature. In addition, in the case of thermal load, an intermediate volume percentage of carbon nanotubes can confer the highest critical temperatures of sandwich shells.

Keywords: CNT-reinforced composite, two-term deflection, sandwich models, thermal load, tangential edge constraint.

1. INTRODUCTION

Due to superior mechanical and thermal properties along with extremely large aspect ratio, carbon nanotubes (CNTs) are used as advanced fillers into isotropic matrix to form carbon nanotube reinforced composite (CNTRC) known as a new class of nanocomposite [1, 2]. The ultimate purpose of developing new materials as CNTs is their application into structural components. Therefore, optimal distribution of CNTs in structures is

a problem of considerable importance. Motivated by the concept of functionally graded material (FGM), Shen [3] proposed the concept of functionally graded carbon nanotube reinforced composite (FG-CNTRC) in which CNTs are reinforced into isotropic matrix in such a way that the volume fraction of CNTs is varied in the thickness direction according to functional rules. Stimulated by this proposal work of Shen, subsequent investigations on static and dynamic responses of FG-CNTRC structures have been performed. Post-buckling analyses of FG-CNTRC cylindrical shells under axial compression and external pressure loads have been carried out by Shen [4,5] employing asymptotic solutions and a higher order shear deformation theory (HSDT). Numerical investigations on buckling and postbuckling behaviors of thin FG-CNTRC cylindrical panels under axial compression and shear loads have been presented by Macias et al. [6,7] in which effective properties of FG-CNTRC are estimated using Eshelby-Mori-Tanaka scheme. Zghal et al. [8] used finite element method to analyze the mechanical buckling behavior of plates and cylindrical panels made of FGM and FG-CNTRC with various boundary conditions. An analytical study of the buckling and postbuckling of simply supported FG-CNTRC toroidal shell segments under external pressure is presented by Tung and Hieu [9] making use of classical shell theory (CST) and thee-term form of deflection. A linear buckling analysis of FG-CNTRC truncated conical shells under lateral pressure was presented by Jam and Kiani [10] employing first order shear deformation theory (FSDT) and differential quadrature method (DQM). Hieu and Tung [11, 12] used the CST and Galerkin method to investigate the nonlinear stability of FG-CNTRC toroidal shell segments and cylindrical shells with elastically restrained edges under lateral pressure in thermal environments.

Since structural components are usually exposed to severe temperature conditions, thermally induced buckling and postbuckling problems of these structures should be addressed. Linear buckling behavior of FG-CNTRC rectangular and skew plates under uniform temperature rise has been studied in works of Kiani and coauthor [13,14] employing Chebyshev-Ritz method and FSDT. Basing on some different plate theories, the thermal postbuckling behavior of FG-CNTRC rectangular plates has been analyzed in works of Shen and Zhang [15] utilizing two-step perturbation technique, Kiani [16] employing Chebyshev-Ritz method, and Tung and Trang [17, 18] making use of Galerkin method. Torabi et al. [19] presented a numerical study on linear buckling of higher order shear deformable FG-CNTRC plates with different shapes under thermal loads. The thermal postbuckling analyses of FG-CNTRC cylindrical panels and shells have been carried out in works of Shen and Xiang [20] and Shen [21], respectively, using asymptotic solutions and a HSDT. Recently, the effects of tangential edge constraints on the thermally induced postbuckling behavior of FG-CNTRC cylindrical panels and cylindrical shells have been analyzed in analytical studies of Trang and Tung [22] utilizing the HSDT and Hieu and Tung [23] using the CST, respectively. Mirzaei and Kiani [24] used the adjacent equilibrium criterion along with discrete singular convolution method to deal with the linear buckling problem of FG-CNTRC truncated conical shells under uniform temperature rise.

Sandwich type structures possess many outstanding characteristics and are widely used in many engineering applications. The generation of advanced nanocomposites such as CNTRC necessitates researches on sandwich structures constituted from these

materials. Shen and Zhu [25] made use of HSDT and a perturbation technique to examine the postbuckling behavior of FG-CNTRC sandwich plates under compressive and thermal loads. By using Ritz method with Chebyshev polynomials as shape functions, Kiani [26] explored the postbuckling behavior of FG-CNTRC sandwich plates with different boundary conditions under uniform temperature rise. A numerical analysis of buckling behavior of FG-CNTRC sandwich shell panels under thermal loads has been carried out in work of Mehar et al. [27] adopting finite element method. In aforementioned works [25–27], sandwich structures are composed of isotropic homogeneous core layer and FG-CNTRC face sheets. Long and Tung [28–30] investigated the postbuckling behavior of sandwich plates and cylindrical panels with FG-CNTRC core layer and face sheets subjected to mechanical and thermal loads. Recently, Foroutan et al. [31] used semi-analytical approach to treat the nonlinear static and dynamic postbuckling responses of sandwich cylindrical panels with an FG-CNTRC core layer taking the hygrothermal and viscoelastic foundation effects into consideration. More recently, Shen et al. [32] assessed the effects of negative Poisson's ratio on the postbuckling behavior of pressure-loaded laminated cylindrical shells made of CNTRC under thermal environments. To the best of authors' knowledge, there is no investigation on the buckling of shear deformable sandwich circular cylindrical shells composed of isotropic homogeneous and FG-CNTRC layers under mechanical and thermal loads.

Recently, Hieu and Tung [33, 34] suggested an effective analytical approach using two-term form of deflection for linear buckling analysis of shear deformable FG-CNTRC cylindrical shells and toroidal shell segments. As an extension of previous work [33], this paper adopts an analytical approach to investigate the buckling behavior of sandwich cylindrical shells comprising CNTRC and homogeneous layers subjected to uniform temperature rise and external lateral pressure. Governing equations are established within the framework of the FSDT. In order to account for practical situations, both temperature dependence of material properties and elasticity of tangential edge constraint are included. Analytical solutions of deflection and stress function are chosen to satisfy simply supported boundary conditions and Galerkin method along with an iteration procedure are adopted to determine the critical loads. After verifying, numerous parametric studies are carried out. Numerical results indicate that tangential edge constraint has significant effect on buckling resistance capacity of the shells. Furthermore, the study reveals that sandwich shell model with thicker CNTRC core layer and homogeneous face sheets can have the highest critical loads.

2. MATERIAL AND STRUCTURAL MODELS

Structural model considered in this study is that a circular cylindrical shell (CCS) of length L, radius R and total thickness h, as shown in Fig. 1. The shell is defined in a coordinate system xyz origin of which is located on the middle surface at one end, x and $y = R\theta$ are longitudinal and circumferential coordinates (θ is circumferential angle), respectively, and z is in the direction of inward normal to the middle surface ($-h/2 \leq z \leq h/2$)
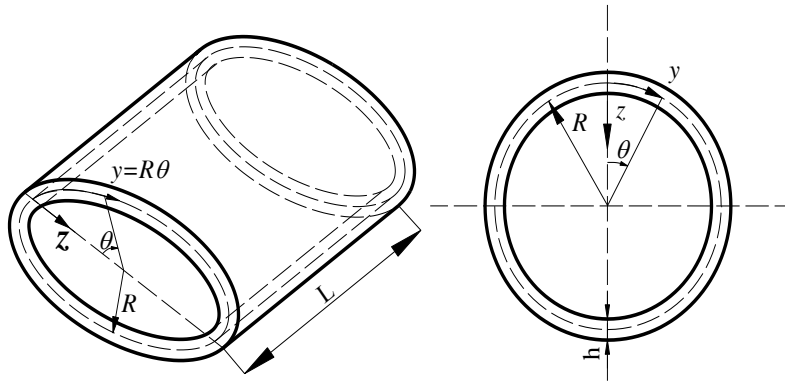
Fig. 1. Geometry and coordinate system of a circular cylindrical shell

The shell is constituted from FG-CNTRC and homogeneous layers. It is assumed that these layers are perfectly bonded and thickness of each face sheet is h_f. This study considers two sandwich models corresponding to CNTRC and homogeneous face sheets and referred to herein as sandwich shells of type A and type B, respectively.

2.1. Sandwich cylindrical shell of type A: Homogeneous core layer and CNTRC face sheets

This type of sandwich shell is a mid-surface symmetric configuration formed from isotropic homogeneous core layer and CNTRC face sheets as shown in Fig. 2.
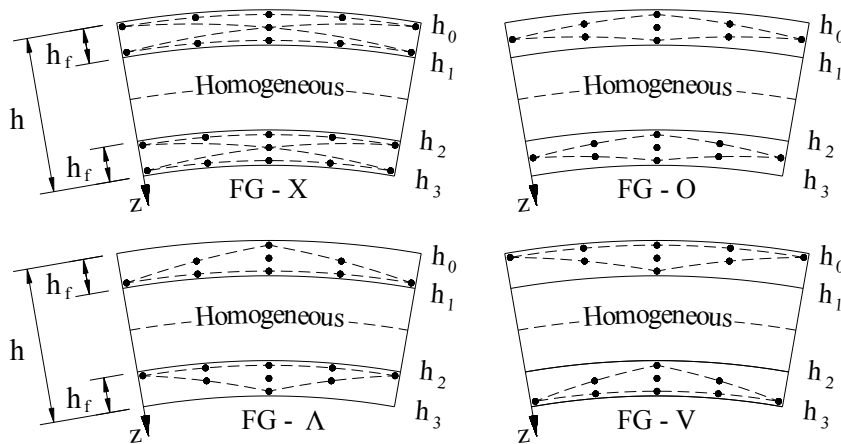

Fig. 2. Functionally graded (FG) types of CNT distribution in sandwich shell of type A

CNTs are reinforced into two face sheets according to distribution types named FG-X, FG-O, FG-Λ and FG-V. Uniform distribution (UD) type is also considered as a special case of CNT distribution. The volume fraction of CNTs, denoted by V_{CNT}, corresponding to these five types of distribution are given in Table 1 in which $h_0 = -h/2, h_1 = -h/2 + h_f, h_2 = h/2 - h_f, h_3 = h/2$, and V_{CNT}^* is total volume fraction of CNTs.

Table 1. Volume fraction $V_{CNT}(z)$ of CNTs in face sheets of sandwich CCS of type A

Distribution type	Outer face sheet ($h_0 \leq z \leq h_1$)	Inner face sheet ($h_2 \leq z \leq h_3$)
UD	V_{CNT}^*	V_{CNT}^*
FG-X	$2\dfrac{|h_0 + h_1 - 2z|}{h_1 - h_0}V_{CNT}^*$	$2\dfrac{|h_2 + h_3 - 2z|}{h_3 - h_2}V_{CNT}^*$
FG-Λ	$2\dfrac{z - h_0}{h_1 - h_0}V_{CNT}^*$	$2\dfrac{h_3 - z}{h_3 - h_2}V_{CNT}^*$
FG-V	$2\dfrac{h_1 - z}{h_1 - h_0}V_{CNT}^*$	$2\dfrac{z - h_2}{h_3 - h_2}V_{CNT}^*$
FG-O	$2\left(1 - \dfrac{|2z - h_0 - h_1|}{h_1 - h_0}\right)V_{CNT}^*$	$2\left(1 - \dfrac{|2z - h_2 - h_3|}{h_3 - h_2}\right)V_{CNT}^*$

2.2. Sandwich cylindrical shell of type B: CNTRC core layer and homogeneous face sheets

As illustrated in Fig. 3, in this sandwich model, cylindrical shell is constituted from a CNTRC core layer and two face sheets made of isotropic homogeneous material properties of which can be different from those of matrix material in CNTRC.
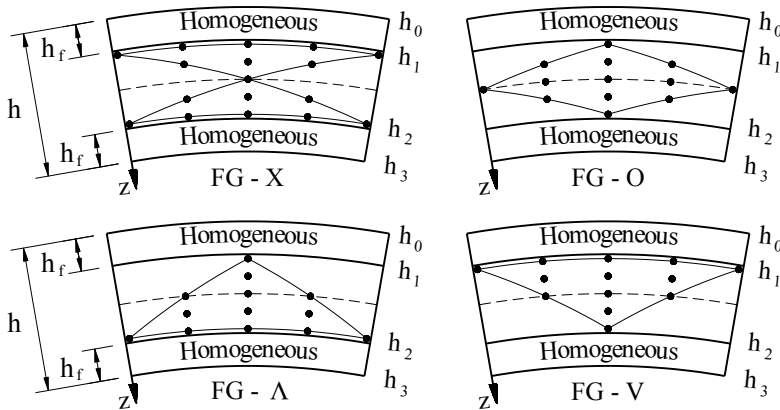

Fig. 3. Functionally graded (FG) types of CNT distribution in sandwich shell of type B

The volume fraction of CNTs in core layer ($h_1 \leq z \leq h_2$) corresponding to above mentioned types of CNT distribution is defined as follows

$$
V_{CNT} = \begin{cases}
V_{CNT}^* & \text{UD} \\[2mm]
4\dfrac{|z|}{h_2 - h_1} V_{CNT}^* & \text{FG-X} \\[2mm]
2\dfrac{z - h_1}{h_2 - h_1} V_{CNT}^* & \text{FG-}\Lambda \\[2mm]
2\dfrac{h_2 - z}{h_2 - h_1} V_{CNT}^* & \text{FG-V} \\[2mm]
2\left(1 - \dfrac{2|z|}{h_2 - h_1}\right) V_{CNT}^* & \text{FG-O}
\end{cases} \tag{1}
$$

For both sandwich models, the effective properties, namely elastic moduli E_{11}, E_{22} and shear modulus G_{12}, of CNTRC are determined using an extended rule of mixture as [3]

$$
E_{11} = \eta_1 V_{CNT} E_{11}^{CNT} + V_m E^m, \tag{2a}
$$

$$
\frac{\eta_2}{E_{22}} = \frac{V_{CNT}}{E_{22}^{CNT}} + \frac{V_m}{E^m}, \tag{2b}
$$

$$
\frac{\eta_3}{G_{12}} = \frac{V_{CNT}}{G_{12}^{CNT}} + \frac{V_m}{G^m}, \tag{2c}
$$

where E_{11}^{CNT}, E_{22}^{CNT} and G_{12}^{CNT} are elastic moduli and shear modulus of CNTs, respectively, E^m and G^m are elastic and shear moduli of isotropic matrix material, respectively, and η_1, η_2, η_3 are CNT efficiency parameters. These parameters are inserted into Eqs. (2) to include size-dependent effects of CNT reinforcements. In addition, $V_m = 1 - V_{CNT}$ denotes the volume fraction of matrix.

Due to weak dependence on position and temperature, effective Poisson's ratio of CNTRC is assumed to be constant and determined using the conventional rule of mixture as [3]

$$
\nu_{12} = V_{CNT}^* \nu_{12}^{CNT} + (1 - V_{CNT}^*) \nu^m, \tag{3}
$$

in which ν_{12}^{CNT} and ν^m are Poisson's ratios of CNT and matrix material, respectively.

In this study, the effective thermal expansion coefficients α_{11} and α_{22} in the longitudinal and transverse directions, respectively, are determined using Schapery model as [20, 21]

$$
\alpha_{11} = \frac{V_{CNT} E_{11}^{CNT} \alpha_{11}^{CNT} + V_m E^m \alpha^m}{V_{CNT} E_{11}^{CNT} + V_m E^m}, \tag{4a}
$$

$$
\alpha_{22} = \left(1 + \nu_{12}^{CNT}\right) V_{CNT} \alpha_{22}^{CNT} + (1 + \nu^m) V_m \alpha^m - \nu_{12} \alpha_{11}, \tag{4b}
$$

where α_{11}^{CNT}, α_{22}^{CNT} and α^m are thermal expansion coefficients of CNT and matrix material, respectively.

Owing to temperature dependence of material properties, the effective properties $E_{11}, E_{22}, G_{12}, \alpha_{11}$ and α_{22} of CNTRC depend on both temperature and position.

3. GOVERNING EQUATIONS

In this study, the sandwich cylindrical shell is assumed to be geometrically perfect and moderately thick, and governing equations are established within the framework of the first order shear deformation theory (FSDT). Based on the FSDT, in-plane strain components $\varepsilon_x, \varepsilon_y, \gamma_{xy}$ and shear deformations γ_{xz}, γ_{yz} at a z distance from the middle surface are expressed as

$$
\begin{pmatrix} \varepsilon_x \\ \varepsilon_y \\ \gamma_{xy} \end{pmatrix} = \begin{pmatrix} \varepsilon_x^0 \\ \varepsilon_y^0 \\ \gamma_{xy}^0 \end{pmatrix} + z \begin{pmatrix} \varepsilon_x^1 \\ \varepsilon_y^1 \\ \gamma_{xy}^1 \end{pmatrix}, \quad \begin{pmatrix} \gamma_{xz} \\ \gamma_{yz} \end{pmatrix} = \begin{pmatrix} \phi_x + w_{,x} \\ \phi_y + w_{,y} \end{pmatrix}, \tag{5}
$$

where

$$
\begin{pmatrix} \varepsilon_x^0 \\ \varepsilon_y^0 \\ \gamma_{xy}^0 \end{pmatrix} = \begin{pmatrix} u_{,x} \\ v_{,y} - w/R \\ u_{,y} + v_{,x} \end{pmatrix}, \quad \begin{pmatrix} \varepsilon_x^1 \\ \varepsilon_y^1 \\ \gamma_{xy}^1 \end{pmatrix} = \begin{pmatrix} \phi_{x,x} \\ \phi_{y,y} \\ \phi_{x,y} + \phi_{y,x} \end{pmatrix}, \tag{6}
$$

in which u, v, w are displacement components in the x, y, z directions, respectively, and ϕ_x, ϕ_y are rotations of a normal to the middle surface with respect to the y, x axes, respectively. Herein, subscript comma indicates the partial derivative with respect to the followed variable, e.g. $w_{,x} = \partial w / \partial x$.

Temperature condition considered in this study is that uniform temperature rise. Specifically, the sandwich shell is exposed to an environment the temperature of which is uniformly raised from reference value T_0 to value T, and difference $\Delta T = T - T_0$ is independent of coordinate variables. Stress components in the shell are computed using constitutive relations as

$$
\begin{pmatrix} \sigma_x \\ \sigma_y \\ \sigma_{xy} \\ \sigma_{xz} \\ \sigma_{yz} \end{pmatrix} = \begin{pmatrix} Q_{11} & Q_{12} & 0 & 0 & 0 \\ Q_{12} & Q_{22} & 0 & 0 & 0 \\ 0 & 0 & Q_{66} & 0 & 0 \\ 0 & 0 & 0 & Q_{44} & 0 \\ 0 & 0 & 0 & 0 & Q_{55} \end{pmatrix} \begin{pmatrix} \varepsilon_x - \alpha_{11} \Delta T \\ \varepsilon_y - \alpha_{22} \Delta T \\ \gamma_{xy} \\ \gamma_{xz} \\ \gamma_{yz} \end{pmatrix}, \tag{7}
$$

where

$$
Q_{11} = \frac{E_{11}}{1 - \nu_{12}\nu_{21}}, \; Q_{22} = \frac{E_{22}}{1 - \nu_{12}\nu_{21}}, \; Q_{12} = \frac{\nu_{21} E_{11}}{1 - \nu_{12}\nu_{21}}, \; Q_{44} = G_{13}, \; Q_{55} = G_{23}, \; Q_{66} = G_{12}, \tag{8}
$$

in CNTRC layers (i.e. $h_0 \leq z \leq h_1$ and $h_2 \leq z \leq h_3$ for sandwich CCS of type A and $h_1 \leq z \leq h_2$ for sandwich CCS of type B), and

$$
E_{11} = E_{22} = E_H, \quad \alpha_{11} = \alpha_{22} = \alpha_H, \quad \nu_{12} = \nu_{21} = \nu_H,
$$

$$
Q_{11} = Q_{22} = \frac{E_H}{1 - \nu_H^2}, \quad Q_{12} = \frac{\nu_H E_H}{1 - \nu_H^2}, \quad Q_{44} = Q_{55} = Q_{66} = \frac{E_H}{2(1 + \nu_H)}, \tag{9}
$$

in isotropic homogeneous layers (i.e. $h_0 \leq z \leq h_1$ and $h_2 \leq z \leq h_3$ for sandwich CCS of type B and $h_1 \leq z \leq h_2$ for sandwich CCS of type A) in which E_H, α_H and ν_H denote Young modulus, thermal expansion coefficient and Poisson ratio of isotropic homogeneous material, respectively.

In-plane force resultants N_x, N_y, N_{xy}, moment resultants M_x, M_y, M_{xy} and transverse shear force resultants Q_x, Q_y are calculated through the stress components and have the form as [28]

$$(N_x, M_x) = (e_{11}, e_{12}) \, \varepsilon_x^0 + \nu_{21} \, (e_{11}, e_{12}) \, \varepsilon_y^0 + (e_{12}, e_{13}) \, \phi_{x,x} + \nu_{21} \, (e_{12}, e_{13}) \, \phi_{y,y} - (e_{11T}, e_{12T}) \, \Delta T,$$

$$(N_y, M_y) = \nu_{12} \, (e_{21}, e_{22}) \, \varepsilon_x^0 + (e_{21}, e_{22}) \, \varepsilon_y^0 + \nu_{12} \, (e_{22}, e_{23}) \, \phi_{x,x} + (e_{22}, e_{23}) \, \phi_{y,y} - (e_{21T}, e_{22T}) \, \Delta T,$$

$$(N_{xy}, M_{xy}) = (e_{31}, e_{32}) \, \gamma_{xy}^0 + (e_{32}, e_{33}) \, (\phi_{x,y} + \phi_{y,x}) \, ,$$

$$Q_x = K_S e_{41} \, (\phi_x + w_{,x}) \, , \quad Q_y = K_S e_{51} \, (\phi_y + w_{,y}) \, ,$$

(10)

where

$$(e_{11}, e_{21}, e_{31}, e_{41}, e_{51}) = \int\limits_{-h/2}^{h/2} (Q_{11}, Q_{22}, Q_{66}, Q_{44}, Q_{55}) \, dz,$$

$$(e_{12}, e_{22}, e_{32}) = \int\limits_{-h/2}^{h/2} (Q_{11}, Q_{22}, Q_{66}) \, z dz, \quad (e_{13}, e_{23}, e_{33}) = \int\limits_{-h/2}^{h/2} (Q_{11}, Q_{22}, Q_{66}) \, z^2 dz,$$

(11)

$$(e_{11T}, e_{12T}) = \int\limits_{-h/2}^{h/2} Q_{11} \, (\alpha_{11} + \nu_{21}\alpha_{22}) \, (1, z) \, dz, \, (e_{21T}, e_{22T}) = \int\limits_{-h/2}^{h/2} Q_{22} \, (\nu_{12}\alpha_{11} + \alpha_{22}) \, (1, z) \, dz,$$

and K_S is shear correction coefficient.

Based on the FSDT, system of equilibrium equations of cylindrical shells includes five equations. After performing mathematical transformations, equilibrium equation of sandwich cylindrical shells is written in the following form [33]

$$a_{11}\phi_{x,xxx} + a_{21}\phi_{x,xyy} + a_{31}\phi_{y,xxy} + a_{41}\phi_{y,yyy} + a_{51}f_{,xxyy} + f_{,yy}w_{,xx} - 2f_{,xy}w_{,xy} + f_{,xx}w_{,yy} + \frac{f_{,xx}}{R} + q = 0,$$

(12)

in which coefficients a_{1i} ($i = 1 \div 5$) has the form as given in the work [28], $f(x, y)$ is a stress function defined as $N_x = f_{,yy}$, $N_y = f_{,xx}$, $N_{xy} = -f_{,xy}$, and q is external lateral pressure uniformly distributed at the outer surface of the shell.

From kinematic relations (6), the strain compatibility equation of a CCS has the form

$$\varepsilon_{x,yy}^0 + \varepsilon_{y,xx}^0 - \gamma_{xy,xy}^0 + \frac{w_{,xx}}{R} = 0.$$

(13)

From Eqs. (10), $\varepsilon_x^0, \varepsilon_y^0, \gamma_{xy}^0$ can be expressed in terms of N_x, N_y, N_{xy}. After that, by substituting the obtained results of $\varepsilon_x^0, \varepsilon_y^0, \gamma_{xy}^0$ into the Eq. (13), the compatibility equation of sandwich cylindrical shells is rewritten in the following form

$$a_{12}f_{,xxxx} + a_{22}f_{,xxyy} + a_{32}f_{,yyyy} + a_{42}\phi_{x,xxx} + a_{52}\phi_{y,xxy} + a_{62}\phi_{y,yyy} + a_{72}\phi_{x,xyy} + \frac{w_{,xx}}{R} = 0,$$

(14)

where the form of coefficients a_{j2} ($j = 1 \div 7$) can be found in the work [28].

4. FORMULATIONS

In this study, the edges of the cylindrical shell are assumed to be simply supported and elastically restrained in the tangential displacement. The associated boundary conditions are expressed as follows

$$w = \phi_y = M_x = 0, \quad N_x = N_{x0} \quad \text{at} \quad x = 0, \ L \tag{15}$$

where N_{x0} is fictitious compressive force resultant at tangentially restrained edges $x = 0$, L. This force resultant is concerned with average end-shortening displacement at boundary edges as [11, 12]

$$N_{x0} = -\frac{c}{2\pi RL} \int\limits_0^{2\pi R} \int\limits_0^L \frac{\partial u}{\partial x} dx dy, \tag{16}$$

in which c is tangential stiffness parameter at edges $x = 0$, L or simply known as the stiffness of elastic springs characterizing tangential edge constraint. It is noticed that Eq. (16) covers all possible cases of in-plane restraints. Concretely, the values of $c = 0$ (i.e. $N_{x0} = 0$), $c \rightarrow \infty$ (i.e. average end-shortening displacement is zero-valued) and $0 < c < \infty$ represent movable, immovable and partially movable edges, respectively.

For circular cylindrical shell, condition of closed periphery must be satisfied. This condition is fulfilled in an average sense in the following

$$\frac{1}{2\pi RL} \int\limits_0^{2\pi R} \int\limits_0^L \frac{\partial v}{\partial y} dx dy = 0. \tag{17}$$

Above boundary conditions are approximately satisfied by assuming the following analytical solutions [33, 34]

$$w(x, y) = W_0 + W_1 \sin \beta_m x \sin \delta_n y, \tag{18a}$$

$$f(x, y) = A_1 \cos 2\beta_m x + A_2 \cos 2\delta_n y + A_3 \sin \beta_m x \sin \delta_n y$$
$$+ A_4 \sin 3\beta_m x \sin \delta_n y - \sigma_{0y} h \frac{x^2}{2} + N_{x0} \frac{y^2}{2}, \tag{18b}$$

$$\phi_x = B_1 \cos \beta_m x \sin \delta_n y, \quad \phi_y = B_2 \sin \beta_m x \cos \delta_n y, \tag{18c}$$

in which W_0 and W_1 are prebuckling uniform deflection and the amplitude of deflection after buckling, respectively, $\beta_m = m\pi/L, \delta_n = n/R$ with m and n are positive integers representing numbers of half and full waves in the longitudinal and circumferential directions, respectively. In addition, σ_{0y} is average circumferential stress and A_i ($i = 1 \div 4$), B_1 and B_2 are coefficients to be determined.

By introducing the solutions (18) into the compatibility equation (14), we obtain

$$A_1 = A_2 = A_4 = 0,$$

$$\left(a_{12}\beta_m^4 + a_{22}\beta_m^2\delta_n^2 + a_{32}\delta_n^4\right) A_3 + \left(a_{42}\beta_m^3 + a_{72}\beta_m\delta_n^2\right) B_1 + \left(a_{52}\beta_m^2\delta_n + a_{62}\delta_n^3\right) B_2 = \frac{\beta_m^2}{R} W_1, \tag{19}$$

Next, by substituting the solutions (18) into the last two of equilibrium equations and performing mathematical procedures as described in previous work [18], we obtain a system of two algebraic equations in terms of A_3, B_1 and B_2. Solving these two equations in combination with the Eq. (19) yields the following result

$$A_3 = A_3^* W_1, \quad B_1 = B_1^* W_1, \quad B_2 = B_2^* W_1, \tag{20}$$

in which the form of coefficients A_3^*, B_1^* and B_2^* is similar to that given in the work [33] and omitted here for the sake of brevity.

Now, substituting the solutions (18) into the equilibrium equation (12) and applying Galerkin method on the whole region of cylindrical shell ($0 \le x \le L, 0 \le y \le 2\pi R$) to the resulting equation, taking into account the condition of non-trivial solution ($W_1 \ne 0$), we obtain the following relations

$$q - \frac{\sigma_{0y}}{R_h} = 0, \tag{21a}$$

$$g_0 + \frac{m^2 \pi^2}{R_h^2 L_R^2} \bar{N}_{x0} - \frac{n^2}{R_h^2} \sigma_{0y} = 0, \tag{21b}$$

where

$$R_h = \frac{R}{h}, \quad L_R = \frac{L}{R}, \quad \bar{N}_{x0} = \frac{N_{x0}}{h}, \tag{22a}$$

$$g_0 = \frac{m^2 \pi^2}{R_h^3 L_R^2} \bar{A}_3^* - \frac{m^2 n^2}{R_h^4 L_R^2} \bar{a}_{51} \pi^2 \bar{A}_3^* - \frac{m^3 \pi^3}{R_h^3 L_R^3} \bar{a}_{11} \bar{B}_1^* - \frac{mn^2 \pi}{R_h^3 L_R} \bar{a}_{21} \bar{B}_1^* - \frac{m^2 n \pi^2}{R_h^3 L_R^2} \bar{a}_{31} \bar{B}_2^* - \frac{n^3}{R_h^3} \bar{a}_{41} \bar{B}_2^*, \tag{22b}$$

in which

$$(\bar{a}_{11}, \bar{a}_{21}, \bar{a}_{31}, \bar{a}_{41}) = \frac{1}{h^3} (a_{11}, a_{21}, a_{31}, a_{41}), \bar{a}_{51} = \frac{a_{51}}{h}, \bar{A}_3^* = \frac{A_3^*}{h^2}, (\bar{B}_1^*, \bar{B}_2^*) = (B_1^*, B_2^*) h. \tag{23}$$

In what follows, the expressions of $\bar{N}_{x0}$ and σ_{0y} will be determined. From Eqs. (6) and (10), the following relations are obtained

$$\frac{\partial u}{\partial x} = \frac{1}{(1 - \nu_{12}\nu_{21})e_{11}e_{21}} \left[e_{21} f_{,yy} - \nu_{21} e_{11} f_{,xx} + (\nu_{12}\nu_{21} e_{11} e_{22} - e_{12} e_{21}) \phi_{x,x} \right.$$
$$\left. + \nu_{21} (e_{11} e_{22} - e_{12} e_{21}) \phi_{y,y} \right] + \frac{e_{21} e_{11T} - \nu_{21} e_{11} e_{21T}}{(1 - \nu_{12}\nu_{21})e_{11}e_{21}} \Delta T, \tag{24a}$$

$$\frac{\partial v}{\partial y} = \frac{1}{(1 - \nu_{12}\nu_{21})e_{11}e_{21}} \left[e_{11} f_{,xx} - \nu_{12} e_{21} f_{,yy} + \nu_{12} (e_{12} e_{21} - e_{11} e_{22}) \phi_{x,x} \right.$$
$$\left. + (\nu_{12}\nu_{21} e_{12} e_{21} - e_{11} e_{22}) \phi_{y,y} \right] + \frac{e_{11} e_{21T} - \nu_{12} e_{21} e_{11T}}{(1 - \nu_{12}\nu_{21})e_{11}e_{21}} \Delta T + \frac{w}{R}. \tag{24b}$$

By placing the solutions (18) into the Eqs. (24) and putting the obtained expressions into the Eqs. (16) and (17), one receives a system of two linear algebraic equations in terms of $\bar{N}_{x0}$ and σ_{0y}. Afterward, by solving these two equations, we obtain the following result

$$\bar{N}_{x0} = -\lambda \frac{\bar{e}_{11}}{R_h} \nu_{21} \bar{W}_0 - \lambda \bar{e}_{11T} \Delta T, \tag{25a}$$

$$\sigma_{0y} = -\nu_{12}\frac{\bar{e}_{21}}{\bar{e}_{11}}\bar{N}_{x0} + \frac{\bar{e}_{21}}{R_h}\left(1 - \nu_{12}\nu_{21}\right)\bar{W}_0 + \left(\bar{e}_{21T} - \nu_{12}\frac{\bar{e}_{21}}{\bar{e}_{11}}\bar{e}_{11T}\right)\Delta T, \qquad (25b)$$

where

$$(\bar{W}_0, \bar{e}_{11}, \bar{e}_{21}, \bar{e}_{11T}, \bar{e}_{21T}) = \frac{1}{h}\left(W_0, e_{11}, e_{21}, e_{11T}, e_{21T}\right), \quad \lambda = \frac{c}{e_{11} + c}, \qquad (26)$$

and λ is a non-dimensional tangential stiffness parameter which will be used in numerical results later. It is noticed that cases of movable ($c = 0$), immovable ($c \to \infty$) and partially movable ($0 < c < \infty$) edges are characterized by values of $\lambda = 0$, $\lambda = 1$ and $0 < \lambda < 1$, respectively.

Subsequently, introduction of $\bar{N}_{x0}$ and σ_{0y} from Eqs. (25) into the Eqs. (21) yields the following expressions

$$\bar{W}_0 = s_{11}q + s_{21}\Delta T, \qquad (27a)$$

$$s_{12} - s_{22}\bar{W}_0 - s_{32}\Delta T = 0, \qquad (27b)$$

where

$$s_{11} = \frac{R_h^4}{s_{31}}, \quad s_{21} = -\frac{R_h^3}{\bar{e}_{11}s_{31}}\left(\bar{e}_{11}\bar{e}_{21T} - \nu_{12}\bar{e}_{21}\bar{e}_{11T} + \lambda\bar{e}_{11T}\nu_{12}\bar{e}_{21}\right),$$

$$s_{31} = R_h^2\bar{e}_{21}\left(1 - \nu_{12}\nu_{21}\right) + \lambda R_h^2 \nu_{12}\nu_{21}\bar{e}_{21},$$

$$s_{12} = g_0, \quad s_{22} = \frac{\bar{e}_{21}}{R_h^3}n^2\left(1 - \nu_{12}\nu_{21}\right) + \lambda\nu_{21}\frac{\bar{e}_{11}}{R_h}\left(\frac{m^2\pi^2}{R_h^2 L_R^2} + \nu_{12}\frac{n^2\bar{e}_{21}}{R_h^2\bar{e}_{11}}\right), \qquad (28)$$

$$s_{32} = \frac{n^2}{R_h^2\bar{e}_{11}}\left(\bar{e}_{11}\bar{e}_{21T} - \nu_{12}\bar{e}_{21}\bar{e}_{11T}\right) + \lambda\bar{e}_{11T}\left(\frac{m^2\pi^2}{R_h^2 L_R^2} + \nu_{12}\frac{n^2\bar{e}_{21}}{R_h^2\bar{e}_{11}}\right).$$

Now, by eliminating the $\bar{W}_0$ from the Eqs. (27), we obtain the following expression

$$q = \frac{s_{12}}{s_{11}s_{22}} - \frac{s_{21}s_{22} + s_{32}}{s_{11}s_{22}}\Delta T. \qquad (29)$$

This is closed-form expression of buckling loads of sandwich cylindrical shells exposed to preexisting thermal environments and subjected to lateral pressure. In another scenario, when the sandwich shell is only subjected to uniform temperature rise, i.e. $q = 0$, the Eq. (29) is rewritten in the form

$$\Delta T = \frac{s_{12}}{s_{21}s_{22} + s_{32}}, \qquad (30)$$

which represents buckling thermal loads of sandwich cylindrical shells. Critical pressures q_{cr} and critical thermal loads ΔT_{cr} are obtained by minimizing the q and ΔT, respectively, with respect to numbers m, n specifying buckling mode. Furthermore, due to temperature dependence of material properties, critical thermal loads are computed using an iteration process.

5. NUMERICAL RESULTS AND DISCUSSION

This section presents numerical results for sandwich circular cylindrical shells (SCCSs) made of nanocomposite and homogeneous layers under lateral pressure and thermal loads. Nanocomposite layer is made of Poly (methyl methacrylate) matrix material, referred to as PMMA, and reinforced by (10, 10) single-walled carbon nanotubes (SWC-NTs). The temperature dependent properties of the PMMA and (10, 10) SWCNTs have been given in many previous works, e.g. [13–15, 20], and are omitted here for the sake of brevity. In addition, CNT efficiency parameters η_j $(j = 1, 2, 3)$ are the same as those given in the works [15,20,21], and it is assumed that $G_{13} = G_{12}, G_{23} = 1.2G_{12}$ [15,16]. The isotropic homogeneous layers are made of Ti-6Al-4V the temperature dependent properties of which are [26]

$$E_H = 122.56 \left(1 - 4.586 \times 10^{-4}T \right) \text{ GPa,}$$

$$\alpha_H = 7.5788 \left(1 + 6.638 \times 10^{-4}T - 3.147 \times 10^{-7}T^2 \right) \times 10^{-6} \text{ K}^{-1}, \quad \nu_H = 0.29, \tag{31}$$

in which $T = T_0 + \Delta T$ (K) and $T_0 = 300$ K is room temperature at which the sandwich shell is assumed to be free from thermal stress. In numerical results, temperature dependent and independent properties will be mentioned to as T-D and T-ID properties, respectively.

Beside the commonly used value $K_S = 5/6$ [10,13,14,16,24,26,33,34], the shear correction coefficient was also suggested to be a value depending on Poisson's ratios of constituent materials in work of Efraim and Eisenberger [35] for functionally graded material (FGM). This suggestion of variable Poisson's rations was also developed in work of Lei et al. [36] for FG-CNTRC. Based on suggestions in previous works [35,36], another value of the K_S is adopted in the present work as the following

$$K_S = K_S^* = \frac{5}{6 - (\nu_{12}^{CNT}V_{CNT}^* + \nu^m V_m)}. \tag{32}$$

5.1. Verification

As mentioned above, there is no investigation on the buckling of CNTRC SCCSs in the literature. Therefore, to verify the proposed work, comparative studies are carried out for special cases of the present work in which the thickness of face sheets in sandwich shell of type B tends to zero and λ receives extreme values. First, the buckling behavior of a shear deformable CNTRC CCS with simply supported and immovable edges under uniform temperature rise is considered. Table 2 shows the results of critical temperatures of the present study corresponding to case of $\lambda = 1$ in comparison with those reported in the works of Shen [21] employing asymptotic solutions, HSDT along with a perturbation technique and of Mirzaei and Kiani [24] adopting adjacent equilibrium criterion, FSDT in conjunction with singular discrete convolution method. It is evident that results of the present work well agree with those in the literature.

As a second example for verification, the buckling behavior of a CNTRC CCS with movable edges under uniform external lateral pressure in thermal environments is considered. The critical pressures of the present work corresponding to case of $\lambda = 0$ are

Table 2. Comparison of critical temperature $T_{cr} = T_0 + \Delta T_{cr}$ (K) of CNTRC CCSs ($R/h = 30, L^2/Rh = 300$) with immovable edges. Numbers in parentheses indicate buckling mode (m, n)

V_{CNT}^*	Reference	UD	FG-X	FG-V	FG-Λ
0.12	Shen [21]	497.44 (1, 3)	507.24 (1, 3)	492.05 (2, 4)	476.30 (2, 4)
	Mirzaei and Kiani [24]	492.24	510.12	483.68	469.43
	Present ($K_S = 5/6$)	497.05 (1, 3)	507.13 (1, 3)	482.78 (2, 4)	466.30 (2, 4)
	Present ($K_S = K_S^*$)	497.05 (1, 3)	507.13 (1, 3)	483.02 (2, 4)	466.42 (2, 4)
0.17	Shen [21]	517.34 (1, 3)	532.03 (1, 3)	507.56 (2, 4)	490.53 (2, 4)
	Mirzaei and Kiani [24]	507.07	532.36	503.30	485.34
	Present ($K_S = 5/6$)	516.36 (1, 3)	529.15 (1, 3)	499.01 (2, 4)	482.04 (2, 4)
	Present ($K_S = K_S^*$)	516.36 (1, 3)	529.15 (1, 3)	499.14 (2, 4)	482.04 (2, 4)
0.28	Shen [21]	474.98 (1, 3)	493.50 (1, 3)	471.41 (2, 4)	462.84 (2, 4)
	Mirzaei and Kiani [24]	474.68	494.06	465.68	457.42
	Present ($K_S = 5/6$)	473.06 (1, 3)	492.37 (1, 3)	465.19 (2, 4)	454.98 (2, 4)
	Present ($K_S = K_S^*$)	473.06 (1, 3)	492.37 (1, 3)	465.31 (2, 4)	455.10 (2, 4)

computed using closed-form expression (29) and compared in Table 3 with results obtained by Shen [5] using the HSDT, asymptotic solutions and a two-step perturbation technique. As can be seen, a very good agreement is achieved in this comparison.

Table 3. Comparison of critical lateral pressures q_{cr} (in kPa) of CNTRC CCSs with movable edges in thermal environments [$R/h = 30, L^2/Rh = 300, V_{CNT}^* = 0.17, (m, n) = (1, 4)$]

T (K)	Reference	UD	FG-X	FG-V	FG-Λ
300	Shen [5]	433.04	484.05	450.14	404.64
	Present ($K_S = 5/6$)	433.18	481.21	450.14	407.99
	Present ($K_S = K_S^*$)	433.29	481.37	450.26	408.08
500	Shen [5]	325.10	365.68	335.58	302.59
	Present ($K_S = 5/6$)	324.74	362.74	335.36	304.24
	Present ($K_S = K_S^*$)	324.83	362.88	335.46	304.31
700	Shen [5]	218.19	248.32	222.37	201.11
	Present ($K_S = 5/6$)	214.39	242.32	218.42	198.67
	Present ($K_S = K_S^*$)	214.47	242.45	218.49	198.72

Above comparisons indicates that results using $K_S = 5/6$ are very slightly smaller than those adopting $K_S = K_S^*$. In other words, difference between results corresponding to two different values of the shear correction coefficient is marginal. Accordingly, in the remainder of this section, the value of $K_S = 5/6$ will be used.

5.2. Buckling analysis of CNTRC SCCSs under thermal load

First, the effects of ratio of thickness of face sheet to total thickness h_f/h and different patterns of CNT distribution in face sheets on critical thermal loads of SCCSs of type A with immovable edges ($\lambda = 1$) are analyzed in Table 4 for both cases of T-D and T-ID properties. It is evident that, for sandwich model with homogeneous core layer and CNTRC face sheets, critical temperatures are considerably reduced when the face sheets become thicker. Among four types of CNT distribution, critical thermal loads corresponding to FG-V and FG-Λ distributions are the highest and lowest, respectively. The difference between critical loads corresponding to different distributions becomes bigger as the h_f/h is larger, i.e. the face sheets are thicker. In addition, Table 4 also indicates that temperature dependence of material properties detrimentally influence on the buckling resistance capacity of CNTRC SCCSs under thermal loads.

Table 4. Effects of h_f/h ratio and type of CNT distribution in face sheets on critical thermal loads ΔT_{cr} (K) of sandwich CCSs of type A ($R/h = 50$, $L^2/Rh = 100$, $V_{CNT}^* = 0.17$, $\lambda = 1$)

Properties	h_f/h	UD	FG-X	FG-V	FG-Λ
T-ID	0.1	772.89 (2, 7)	773.73 (2, 7)	776.69 (2, 7)	770.61 (2, 7)
	0.15	683.51 (2, 7)	684.90 (2, 7)	691.52 (2, 7)	677.68 (2, 7)
	0.2	607.91 (2, 7)	610.09 (2, 7)	621.44 (1, 6)	596.86 (2, 7)
	0.5	196.63 (1, 5)	207.20 (1, 5)	228.65 (1, 5)	171.14 (1, 5)
T-D	0.1	652.88 (2, 7)	653.01 (2, 7)	656.21 (2, 7)	649.68 (2, 7)
	0.15	572.19 (2, 7)	572.81 (2, 7)	579.58 (2, 7)	565.55 (2, 7)
	0.2	502.33 (2, 7)	503.56 (2, 7)	501.96 (1, 6)	491.02 (2, 7)
	0.5	137.64 (1, 5)	143.54 (1, 5)	155.96 (1, 5)	121.77 (1, 5)

Numbers in the parentheses indicate buckling mode (m, n).

Next, the effects of total volume fraction V_{CNT}^* of CNTs and degree of tangential edge constraint λ on the critical thermal loads ΔT_{cr} of CNTRC SCCSs of type A ($h_f/h = 0.2$) are examined in Table 5. It is interesting to notice that critical thermal loads are slightly decreased when V_{CNT}^* is increased from 0.12 to 0.28 in the case of T-ID properties. Unlike this trend, when T-D properties are taken into consideration, the critical load corresponding to case of $V_{CNT}^* = 0.17$ is the highest and critical loads corresponding to values of $V_{CNT}^* = 0.12$ and $V_{CNT}^* = 0.28$ are almost coincident. These analyses explore that for thermally loaded SCCSs an average percentage of CNT volume in face sheets can confer the best capacity of buckling resistance. Furthermore, results in Table 5 also find that critical thermal loads and difference between predictions corresponding to T-D and T-ID cases are lowered when parameter λ become larger, i.e. edges are restrained more severely.

Subsequent numerical result is shown in Fig. 4 evaluating the effects of h_f/h ratio and various patterns of CNT distribution in core layer on critical thermal loads of CNTRC SCCSs of type B with immovable edges. As can be observed, critical thermal loads are

Table 5. Effects of V_{CNT}^* and degree of tangential edge constraint on critical thermal loads ΔT_{cr} (K) of sandwich CCSs of type A $[R/h = 50, L^2/Rh = 200, \text{FG-V}, h_f/h = 0.2, (m, n) = (2, 7)]$

Properties	V_{CNT}^*	λ				
		0.6	0.7	0.8	0.9	1.0
T-D	0.12	1016.0	871.2	762.5	677.9	610.4
	0.17	1032.2	885.0	774.7	688.8	620.2
	0.28	1016.3	871.3	762.5	677.9	610.3
T-ID	0.12	823.8	713.4	627.9	561.1	507.9
	0.17	801.9	698.6	617.1	552.8	501.0
	0.28	763.1	665.9	588.8	527.7	478.6

rapidly enhanced when the h_f/h ratio increases to a definite value (about $h_f/h = 0.3$ in this illustration) and then slightly increased and decreased for cases of T-D and T-ID properties, respectively. This analysis suggests that sandwich model with a CNTRC core layer and relatively thin homogeneous face sheets can bring the sandwich shell to the best thermal buckling resistance capacity. Fig. 4 also indicates that FG-X type of CNT distribution in core layer induces the highest critical temperature for SCCS of type B.
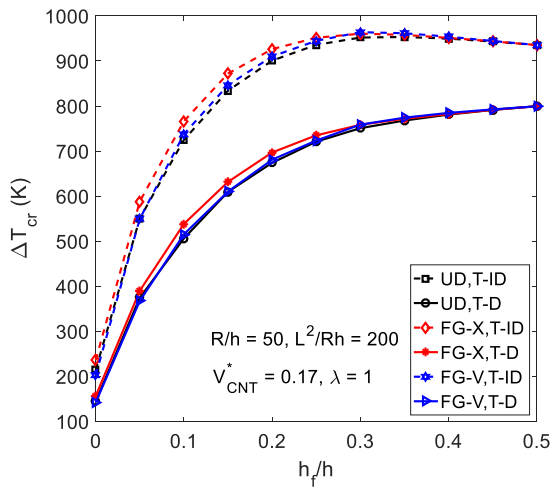

Fig. 4. Effects of h_f/h ratio and CNT distribution on critical thermal loads of SCCSs of type B with immovable edges
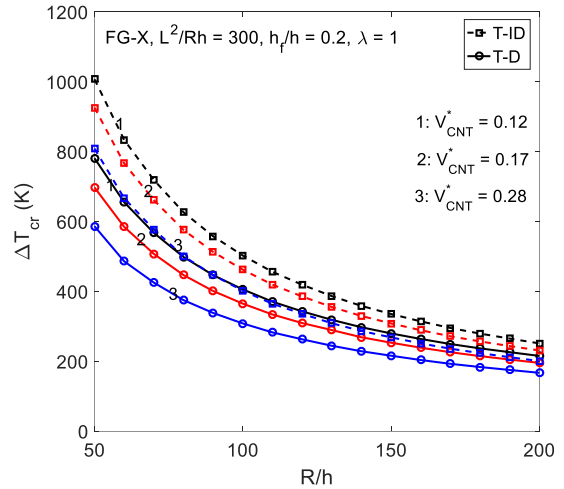
Fig. 5. Effects of CNT volume fraction and R/h ratio on critical thermal loads of SCCSs of type B with immovable edges

Final illustrative example in this subsection is displayed in Fig. 5 considering the effects of total volume fraction V_{CNT}^* of CNT in core layer and radius-to-thickness R/h ratio on critical thermal loads ΔT_{cr} of SCCSs of type B with immovable edges. It is recognized from Fig. 5 that critical thermal loads are reduced due to increase in the volume fraction of CNTs for both cases of T-D and T-ID properties. In other words, high percentage of

CNTs in core layer makes the thermal buckling resistance capacity of SCCSs of type B weakened. In addition, it is clear that critical thermal loads become significantly lower and harmful influences of T-D properties are more benign for larger values of R/h ratio, namely thinner shells.

5.3. Buckling analysis of CNTRC SCCSs under lateral pressure

This subsection presents some numerical results for buckling analysis of CNTRC SCCSs of types A and B under uniform external lateral pressure in thermal environments. Table 6 shows the effects of volume fraction V_{CNT}^* of CNTs, h_f/h ratio and type of CNT distribution in face sheets on critical loads of CNTRC SCCSs of type A with movable edges under external pressure at room temperature. Obviously, critical pressures are increased and decreased by virtue of increases in V_{CNT}^* and h_f/h, respectively. More specifically, positive effect of high percentage of CNT reinforcement is more pronounced for thicker face sheets. Basically, the type of CNT distribution in face sheets has slight effect on critical pressures and FG-V distribution yields the highest critical pressures.

Table 6. Critical loads q_{cr} (MPa) of sandwich CCSs of type A with movable edges under external pressure at room temperature ($R/h = 30$, $T = 300$ K, $\lambda = 0$, $L^2/Rh = 100$)

V_{CNT}^*	h_f/h	UD	FG-X	FG-V	FG-O	FG-Λ
0.12	0.1	7.2260 (1, 5)	7.2270 (1, 5)	7.2320 (1, 5)	7.2267 (1, 5)	7.2217 (1, 5)
	0.2	3.9746 (1, 5)	3.9771 (1, 5)	3.9943 (1, 5)	3.9748 (1, 5)	3.9576 (1, 5)
	0.3	1.7857 (1, 6)	1.7912 (1, 6)	1.8198 (1, 6)	1.7844 (1, 6)	1.7559 (1, 6)
0.17	0.1	7.4150 (1, 5)	7.4184 (1, 5)	7.4271 (1, 5)	7.4179 (1, 5)	7.4091 (1, 5)
	0.2	4.2901 (1, 5)	4.2972 (1, 5)	4.3274 (1, 5)	4.2931 (1, 5)	4.2630 (1, 5)
	0.3	2.1198 (1, 6)	2.1346 (1, 6)	2.1893 (1, 6)	2.1216 (1, 6)	2.0675 (1, 6)
0.28	0.1	7.6225 (1, 5)	7.6364 (1, 5)	7.6526 (1, 5)	7.6355 (1, 5)	7.6194 (1, 5)
	0.2	4.4979 (1, 6)	4.5314 (1, 6)	4.5879 (1, 6)	4.5239 (1, 6)	4.4682 (1, 6)
	0.3	2.3536 (1, 6)	2.4026 (1, 6)	2.5093 (1, 6)	2.3773 (1, 6)	2.2730 (1, 6)

Numbers in the parentheses indicate buckling mode (m, n).

Subsequently, the influences of environment temperature T, geometry ratio L^2/Rh and pattern of CNT distribution in core layer on critical pressures of the SCCSs of type B with movable edges ($\lambda = 0$) are examined in Table 7. As can be seen, critical pressures corresponding to FG-V and FG-Λ distribution patterns are the highest and lowest, respectively. This means that SCCSs the inner and outer surfaces of which are enriched by CNTs have the strongest and weakest capacities of external pressure resistance, respectively. Table 7 also demonstrates that critical pressures are slightly and significantly reduced when temperature T and L^2/Rh ratio are enhanced, respectively.

Table 7. Critical loads q_{cr} (MPa) of sandwich CCSs of type B under external pressure with movable edges in thermal environments ($R/h = 30$, $V_{CNT}^* = 0.17$, $\lambda = 0$, $h_f/h = 0.2$)

T (K)	L^2/Rh	UD	FG-X	FG-V	FG-O	FG-Λ
300	100	9.7924 (1, 5)	9.8211 (1, 5)	9.9266 (1, 5)	9.7679 (1, 5)	9.6566 (1, 5)
	200	6.6112 (1, 4)	6.6255 (1, 4)	6.7060 (1, 4)	6.5997 (1, 4)	6.5175 (1, 4)
	300	5.6836 (1, 4)	5.6938 (1, 4)	5.7350 (1, 4)	5.6757 (1, 4)	5.6345 (1, 4)
400	100	9.2766 (1, 5)	9.3033 (1, 5)	9.4061 (1, 5)	9.2536 (1, 5)	9.1447 (1, 5)
	200	6.2711 (1, 4)	6.2843 (1, 4)	6.3628 (1, 4)	6.2605 (1, 4)	6.1801 (1, 4)
	300	5.3870 (1, 4)	5.3962 (1, 4)	5.4366 (1, 4)	5.3799 (1, 4)	5.3392 (1, 4)

Numbers in the parentheses indicate buckling mode (m, n).

Next, the effects of tangential edge constraint and elevated temperature on the critical pressures of SCCSs of types A and B are depicted in Figs. 6 and 7, respectively. Evidently, critical pressures are substantially decreased by virtue of increases in temperature T and/or parameter λ. More specifically, the enhancement of degree of tangential edge constraint induces the slight and considerable decreases in critical pressures at low and high levels of temperature, respectively. This is explained by the fact that thermal compressive stresses at edges are higher as the edges are more rigorously restrained.
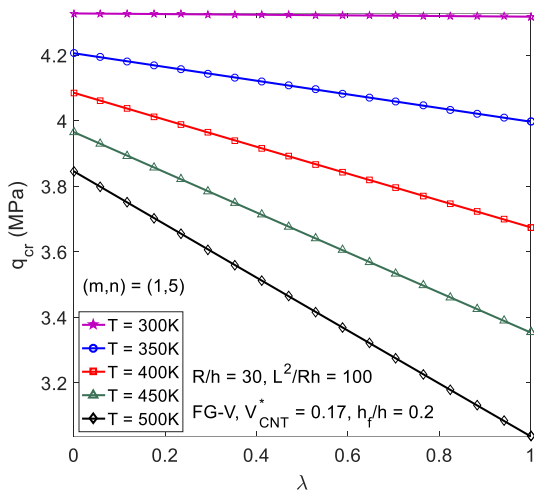

Fig. 6. Combined effects of tangential edge constraint and elevated temperature on critical pressures of sandwich CCSs of type A
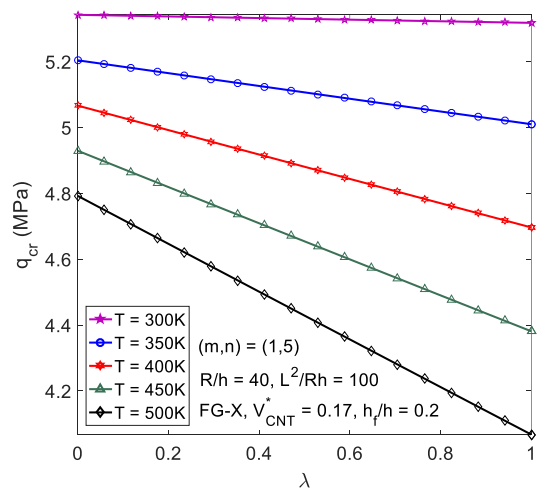
Fig. 7. Combined effects of tangential edge constraint and elevated temperature on critical pressures of sandwich CCSs of type B

Finally, Figs. 8 sketches the variation of critical pressures of SCCSs of type B with movable edges versus change of thickness of face sheets and volume fraction of CNTs.

It is clear that the buckling resistance capability of SCCSs is stronger when the homogeneous face sheets becomes thicker. In contrary to case of thermal load, critical loads of CNTRC SCCSs under external pressure are enhanced when the percentage of CNT volume V^*_{CNT} in core layer is higher. Furthermore, beneficial effect of V^*_{CNT} on critical pressure is of less significance with higher value of h_f/h ratio.
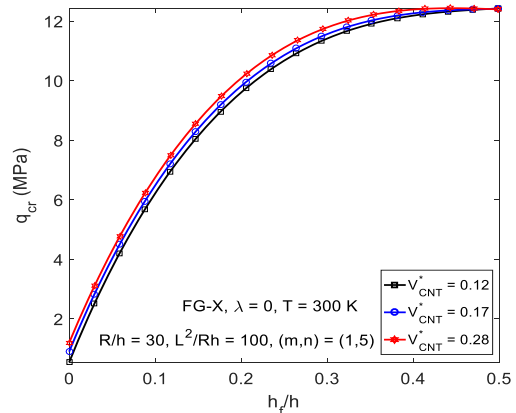

Fig. 8. Effects of thickness of face sheets and CNT volume fraction on critical pressures of sandwich CCSs of type B

6. CONCLUDING REMARKS

Based on an effective analytical approach, the buckling behavior of shear deformable sandwich cylindrical shells comprising CNTRC and homogenous layers subjected to uniform temperature rise and external lateral pressure has been analyzed. Both temperature dependence of material properties and elasticity of tangential constraint of edges are taken into consideration. Above obtained results suggests the following remarks:

1. Buckling resistance capacity of sandwich shells under thermal and pressure loads is weakened when boundary edges are more severely restrained. For pressure-loaded shells, critical pressures are slightly and considerably decreased by increase in degree of tangential edge constraint at low and high temperatures, respectively.

2. Critical loads of pressure-loaded shells are enhanced by increase in CNT volume fraction. In contrast, a small percentage of CNT volume can confer the strongest capacity of buckling resistance of thermally loaded CNTRC SCCSs.

3. Sandwich shell model constituted from a thicker CNTRC core layer and homogeneous face sheets can be an advanced sandwich model with many outstanding characteristics and potential applications.

ACKNOWLEDGMENT

REFERENCES

[1] E. T. Thostenson, Z. Ren, and T.-W. Chou. Advances in the science and technology of carbon nanotubes and their composites: a review. *Composites Science and Technology*, **61**, (2001), pp. 1899–1912. https://doi.org/10.1016/s0266-3538(01)00094-x.

[2] J. N. Coleman, U. Khan, W. J. Blau, and Y. K. Gun'ko. Small but strong: A review of the mechanical properties of carbon nanotube–polymer composites. *Carbon*, **44**, (2006), pp. 1624–1652. https://doi.org/10.1016/j.carbon.2006.02.038.

[3] H.-S. Shen. Nonlinear bending of functionally graded carbon nanotube-reinforced composite plates in thermal environments. *Composite Structures*, **91**, (2009), pp. 9–19. https://doi.org/10.1016/j.compstruct.2009.04.026.

[4] H.-S. Shen. Postbuckling of nanotube-reinforced composite cylindrical shells in thermal environments, Part I: Axially-loaded shells. *Composite Structures*, **93**, (2011), pp. 2096–2108. https://doi.org/10.1016/j.compstruct.2011.02.011.

[5] H.-S. Shen. Postbuckling of nanotube-reinforced composite cylindrical shells in thermal environments, part II: Pressure-loaded shells. *Composite Structures*, **93**, (2011), pp. 2496–2503. https://doi.org/10.1016/j.compstruct.2011.04.005.

[6] E. García-Macías, L. Rodriguez-Tembleque, R. Castro-Triguero, and A. Sáez. Buckling analysis of functionally graded carbon nanotube-reinforced curved panels under axial compression and shear. *Composites Part B: Engineering*, **108**, (2017), pp. 243–256. https://doi.org/10.1016/j.compositesb.2016.10.002.

[7] E. García-Macías, L. Rodríguez-Tembleque, R. Castro-Triguero, and A. Sáez. Eshelby-Mori-Tanaka approach for post-buckling analysis of axially compressed functionally graded CNT/polymer composite cylindrical panels. *Composites Part B: Engineering*, **128**, (2017), pp. 208–224. https://doi.org/10.1016/j.compositesb.2017.07.016.

[8] S. Zghal, A. Frikha, and F. Dammak. Mechanical buckling analysis of functionally graded power-based and carbon nanotubes-reinforced composite plates and curved panels. *Composites Part B: Engineering*, **150**, (2018), pp. 165–183. https://doi.org/10.1016/j.compositesb.2018.05.037.

[9] H. V. Tung and P. T. Hieu. Nonlinear buckling of CNT-reinforced composite toroidal shell segment surrounded by an elastic medium and subjected to uniform external pressure. *Vietnam Journal of Mechanics*, **40**, (2018), pp. 285–301. https://doi.org/10.15625/0866-7136/12397.

[10] J. Jam and Y. Kiani. Buckling of pressurized functionally graded carbon nanotube reinforced conical shells. *Composite Structures*, **125**, (2015), pp. 586–595. https://doi.org/10.1016/j.compstruct.2015.02.052.

[11] P. T. Hieu and H. V. Tung. Thermomechanical postbuckling of pressure-loaded CNT-reinforced composite cylindrical shells under tangential edge constraints and various temperature conditions. *Polymer Composites*, **41**, (2019), pp. 244–257. https://doi.org/10.1002/pc.25365.

[12] P. T. Hieu and H. V. Tung. Thermomechanical nonlinear buckling of pressure-loaded carbon nanotube reinforced composite toroidal shell segment surrounded by an elastic medium with tangentially restrained edges. *Proceedings of the Institution of Mechanical Engineers, Part C: Journal of Mechanical Engineering Science*, **233**, (2018), pp. 3193–3207. https://doi.org/10.1177/0954406218802942.

[13] M. Mirzaei and Y. Kiani. Thermal buckling of temperature dependent FG-CNT reinforced composite plates. *Meccanica*, **51**, (2015), pp. 2185–2201. https://doi.org/10.1007/s11012-015-0348-0.

[14] Y. Kiani. Thermal buckling of temperature-dependent FG-CNT-reinforced composite skew plates. *Journal of Thermal Stresses*, **40**, (2017), pp. 1442–1460. https://doi.org/10.1080/01495739.2017.1336742.

[15] H.-S. Shen and C.-L. Zhang. Thermal buckling and postbuckling behavior of functionally graded carbon nanotube-reinforced composite plates. *Materials & Design*, **31**, (2010), pp. 3403–3411. https://doi.org/10.1016/j.matdes.2010.01.048.

[16] Y. Kiani. Thermal post-buckling of FG-CNT reinforced composite plates. *Composite Structures*, **159**, (2017), pp. 299–306. https://doi.org/10.1016/j.compstruct.2016.09.084.

[17] H. V. Tung. Thermal buckling and postbuckling behavior of functionally graded carbon-nanotube-reinforced composite plates resting on elastic foundations with tangential-edge restraints. *Journal of Thermal Stresses*, **40**, (2016), pp. 641–663. https://doi.org/10.1080/01495739.2016.1254577.

[18] H. V. Tung and L. T. N. Trang. Thermal postbuckling of shear deformable CNT-reinforced composite plates with tangentially restrained edges and temperature-dependent properties. *Journal of Thermoplastic Composite Materials*, **33**, (2018), pp. 97–124. https://doi.org/10.1177/0892705718804588.

[19] J. Torabi, R. Ansari, and R. Hassani. Numerical study on the thermal buckling analysis of CNT-reinforced composite plates with different shapes based on the higher-order shear deformation theory. *European Journal of Mechanics - A/Solids*, **73**, (2019), pp. 144–160. https://doi.org/10.1016/j.euromechsol.2018.07.009.

[20] H.-S. Shen and Y. Xiang. Thermal postbuckling of nanotube-reinforced composite cylindrical panels resting on elastic foundations. *Composite Structures*, **123**, (2015), pp. 383–392. https://doi.org/10.1016/j.compstruct.2014.12.059.

[21] H.-S. Shen. Thermal buckling and postbuckling behavior of functionally graded carbon nanotube-reinforced composite cylindrical shells. *Composites Part B: Engineering*, **43**, (2012), pp. 1030–1038. https://doi.org/10.1016/j.compositesb.2011.10.004.

[22] L. T. N. Trang and H. V. Tung. Thermally induced postbuckling of higher order shear deformable CNT-reinforced composite flat and cylindrical panels resting on elastic foundations with elastically restrained edges. *Mechanics Based Design of Structures and Machines*, (2020), pp. 1–24. https://doi.org/10.1080/15397734.2020.1785312.

[23] P. T. Hieu and H. V. Tung. Thermal buckling and postbuckling of CNT-reinforced composite cylindrical shell surrounded by an elastic medium with tangentially restrained edges. *Journal of Thermoplastic Composite Materials*, **34**, (2019), pp. 861–883. https://doi.org/10.1177/0892705719853611.

[24] M. Mirzaei and Y. Kiani. Thermal buckling of temperature dependent FG-CNT reinforced composite conical shells. *Aerospace Science and Technology*, **47**, (2015), pp. 42–53. https://doi.org/10.1016/j.ast.2015.09.011.

[25] H.-S. Shen and Z. H. Zhu. Postbuckling of sandwich plates with nanotube-reinforced composite face sheets resting on elastic foundations. *European Journal of Mechanics - A/Solids*, **35**, (2012), pp. 10–21. https://doi.org/10.1016/j.euromechsol.2012.01.005.

[26] Y. Kiani. Thermal post-buckling of temperature dependent sandwich plates with FG-CNTRC face sheets. *Journal of Thermal Stresses*, **41**, (2018), pp. 866–882. https://doi.org/10.1080/01495739.2018.1425645.

[27] K. Mehar, S. K. Panda, Y. Devarajan, and G. Choubey. Numerical buckling analysis of graded CNT-reinforced composite sandwich shell structure under thermal loading. *Composite Structures*, **216**, (2019), pp. 406–414. https://doi.org/10.1016/j.compstruct.2019.03.002.

[28] V. T. Long and H. V. Tung. Thermal postbuckling behavior of CNT-reinforced composite sandwich plate models resting on elastic foundations with tangentially restrained edges and temperature-dependent properties. *Journal of Thermoplastic Composite Materials*, **33**, (2019), pp. 1396–1428. https://doi.org/10.1177/0892705719828789.

[29] V. T. Long and H. V. Tung. Thermomechanical postbuckling behavior of CNT-reinforced composite sandwich plate models resting on elastic foundations with elastically restrained unloaded edges. *Journal of Thermal Stresses*, **42**, (2019), pp. 658–680. https://doi.org/10.1080/01495739.2019.1571972.

[30] H. V. Tung and V. T. Long. Buckling and postbuckling of CNT-reinforced composite sandwich cylindrical panels subjected to axial compression in thermal environments. *Vietnam Journal of Mechanics*, **41**, (2019), pp. 217–231. https://doi.org/10.15625/0866-7136/13673.

[31] K. Foroutan, E. Carrera, and H. Ahmadi. Static and dynamic hygrothermal postbuckling analysis of sandwich cylindrical panels with an FG-CNTRC core surrounded by nonlinear viscoelastic foundations. *Composite Structures*, **259**, (2021). https://doi.org/10.1016/j.compstruct.2020.113214.

[32] H.-S. Shen, C. Li, and X.-H. Huang. Assessment of negative Poisson's ratio effect on the postbuckling of pressure-loaded FG-CNTRC laminated cylindrical shells. *Mechanics Based Design of Structures and Machines*, (2021). https://doi.org/10.1080/15397734.2021.1880934.

[33] P. T. Hieu and H. V. Tung. Thermal and thermomechanical buckling of shear deformable FG-CNTRC cylindrical shells and toroidal shell segments with tangentially restrained edges. *Archive of Applied Mechanics*, **90**, (2020), pp. 1529–1546. https://doi.org/10.1007/s00419-020-01682-7.

[34] P. T. Hieu and H. V. Tung. Buckling of shear deformable FG-CNTRC cylindrical shells and toroidal shell segments under mechanical loads in thermal environments. *ZAMM - Journal of Applied Mathematics and Mechanics / Zeitschrift für Angewandte Mathematik und Mechanik*, **100**, (2020). https://doi.org/10.1002/zamm.201900243.

[35] E. Efraim and M. Eisenberger. Exact vibration analysis of variable thickness thick annular isotropic and FGM plates. *Journal of Sound and Vibration*, **299**, (2007), pp. 720–738. https://doi.org/10.1016/j.jsv.2006.06.068.

[36] Z. X. Lei, K. M. Liew, and J. L. Yu. Buckling analysis of functionally graded carbon nanotube-reinforced composite plates using the element-free kp-Ritz method. *Composite Structures*, **98**, (2013), pp. 160–168. https://doi.org/10.1016/j.compstruct.2012.11.006.